Fuel 300 (2021) 120980

Contents lists available at ScienceDirect

Fuel

journal homepage: www.elsevier.com/locate/fuel

Full Length Article

Pyrolysis of petroleum sludge under non-isothermal conditions: Thermal decomposition behavior, kinetics, thermodynamics, and evolved gas analysis

Gamzenur Özsin [a], Esin Apaydın-Varol [b,*], Murat Kılıç [b], Ayşe E. Pütün [c], Ersan Pütün [d]

[a] Bilecik Şeyh Edebali University, Chemical Engineering Department, Bilecik 11230, Turkey
[b] Eskişehir Technical University, Chemical Engineering Department, Eskişehir 26555, Turkey
[c] Anadolu University, Chemical Engineering Department, Eskişehir 26555, Turkey
[d] Anadolu University, Materials Science and Engineering Department, Eskişehir 26555, Turkey

ARTICLE INFO

Keywords:
Petroleum sludge
Pyrolysis
Kinetics
Thermodynamics
TGA/FT-IR

ABSTRACT

Pyrolysis of petroleum sludge is considered as a promising way for energy production from solid waste of petroleum refineries and the ability to predict the thermal decomposition behavior of such processes is necessary for modeling, optimization, and control of the pyrolysis reactors. Therefore, this work focused on developing and applying a systematic methodology for the calculation of kinetics and thermodynamics of the oil sludge pyrolysis and investigation of evolved gases. Thermograms at different heating rates demonstrated that the pyrolysis reactions could be considered under three zones; i) moisture and low molecular weight hydrocarbon volatilization, ii) active pyrolysis, and iii) high-temperature carbonization. During active pyrolysis, two decomposition stages were obtained by deconvolution using the Asym2sig function, which indicated the occurrence of multiple reactions. The average activation energies, calculated by the *iso*-conversional models, ranged in 106.3–112.7 kJ.mol^{-1} and 200.9–207.6 kJ.mol^{-1} for the first and second pyrolysis stages, respectively. Flynn-Wall-Ozawa and Friedman models showed the best consistency between the experimental and predicted values. The average pre-exponential factors were estimated as 9.79×10^{6} s^{-1} and 1.91×10^{12} s^{-1} for these subsequent sub-stages. Furthermore, enthalpy, Gibbs free energy, and entropy changes were estimated together with monitoring emission profiles of the released gases from the sludge during pyrolysis by coupling TGA with an FT-IR spectrometer. The reported kinetic, thermodynamic parameters and findings on evolved gases can expand the use of this residue in refinery applications, consisting of a great attempt toward its valorization.

1. Introduction

During the production of petroleum-based products through refinery processes, considerable amount of oily waste as sludge is generated. It is estimated that more than 60 million tons of oil sludge can be produced annually and more than 1 billion tons of sludge has been accumulated worldwide [1]. There are several sources of petroleum sludge-like oil–water separators, wastewater treatment units, and cleaning wastes of process instruments. In particular, bottom sections of the storage tanks are the main sources of sludge which have time-consuming, labor-intensive disposal problems during the periodically cleaning procedures [2,3]. Crude oil sludge has been regarded as a toxic and hazardous substance since it is a stable emulsion that contains many chemical species including benzene, toluene, ethyl-benzene, xylene, polycyclic aromatic hydrocarbons, and heavy metals [4,5]. Moreover, some mineral admixtures that consist of surface soil, drilling mud residues, and fine suspended particles may also exist in their composition [6]. Therefore, disposal and recovery technologies of petroleum sludge have attracted increasing attention due to environmental regulations and requirements for technological progress in enterprises [7,8]. To this end, a variety of oil sludge utilization approaches have been developed, and these include physical (filtering, settling, or centrifuging), chemical (extraction, solidification), and biological (microbiological decomposition, bio-thermal decomposition) techniques [9]. By employing these methods, toxic substances can be reduced or eliminated and hazardous environmental effects can be mitigated. However, many of the aforementioned methods are considered disadvantageous due to their high cost, low efficiency, secondary pollution generation, and long treatment periods [10].

* Corresponding author.
E-mail address: eapaydin@eskisehir.edu.tr (E. Apaydın-Varol).

https://doi.org/10.1016/j.fuel.2021.120980
Received 19 January 2021; Received in revised form 1 April 2021; Accepted 1 May 2021
Available online 10 May 2021

Nomenclature

List of Symbols

A	Pre-exponential factor (s^{-1})
e	Neper number (2.7183)
E_a	Activation energy (kJ mol^{-1})
h	Planck constant (6.626×10^{-34} J s)
k	Reaction rate constant
k_B	Boltzmann constant (1.381×10^{-23} J K^{-1})
k(T)	Temperature function
L	Length of the molecular unit (m)
R	Universal gas constant (8.3144×10^{-3} kJ mol^{-1} K^{-1})
R_p	Pyrolysis reactivity index
R^2	Coefficient of determination (R-squared)
Adj.R^2	Adjusted coefficient of determination
S_{BET}	Surface area calculated by Brunauer-Emmet-Teller Equation (m^2 g^{-1})
SD	Standard deviation
t	Time (s)
T	Temperature (K)
T_i	Temperature at which the decomposition is started (K)
T_{max}	Temperature at which the highest decomposition rate is observed (K)
T_f	Temperature at which the decomposition is completed (K)
T_p	Average peak temperature (K)
w_o	Mass at the initial stage of the reaction (mg)
w_f	Mass at the final stage of the reaction (mg)
w_t	Mass at time t (mg)
f(α)	Fractional conversion function
g(α)	Integrated form of reaction model
p(u)	Temperature integral
α	Fractional conversion
β	Heating rate (K min^{-1})
ρ	Density of the solid (kg m^{-3})
χ	Transmission factor
$\bar{x}$	Mean value
$\Delta G^{\neq}$	Gibbs free energy change (kJ mol^{-1})
$\Delta H^{\neq}$	Enthalpy change (kJ mol^{-1})
$\Delta S^{\neq}$	Entropy change (J mol^{-1} K^{-1})

Recovery of hydrocarbons from oil sludge would yield substantial environmental and economic benefits, since these materials are a potential source of energy and chemical feedstock due to their high carbon and hydrogen contents [11–14]. Several researchers have reported that thermochemical conversion methods may be an ideal technique to recover value-added products such as hydrocarbons and synthesis gas from oil sludge. By pyrolytic degradation of oil sludge, it is possible to recover more than 80 wt% of the oil as paraffins, olefins, and aromatics as a liquid product [15–17]. Furthermore, enhancement of the rate of conversion, increasing liquid product yield, upgrading the quality of liquid product may also be achieved in the presence of some additives [18–22]. Although pyrolysis technology offers a practical and alternative method for resource utilization of petroleum sludges [23], describing pyrolytic decomposition is challenging. This is because, pyrolysis is comprised of many primary and secondary parallel reactions, as well as competitive reactions [24]. Petroleum sludge is also a heterogeneous substance that has different compositions depending on the process conditions. For studying the solid-state decomposition reactions of such complex materials, thermogravimetric analysis (TGA) is a useful technique due to its sensitivity towards thermally stimulated processes. Therefore, TGA has been often used to describe the thermochemical behaviors and kinetics of waste materials with complex structures such as municipal, industrial, and agricultural wastes [25–31].

In view of the considerations given above, the aim of this study is to investigate the pyrolytic decomposition of crude oil sludge through TGA/FT-IR analysis. Recently, few studies have been reported on the pyrolysis characteristics of petroleum sludge obtained from API separators [32], crude oil storage tanks [33], and wastewater treatment plants of refineries [34] through TG-MS. Moreover, Cheng et al. carried out thermal analysis and kinetics of oil sludge considering the evaporation stage of the sludge and establishing the relationship between the peak distribution and the surface properties of the oil sludge particles [35]. However, it should be noted that comprehensive kinetic and thermodynamic analyses of petroleum sludge pyrolysis together with evolved gas analysis were performed for the first time in this study. Considering the above-discussed gap in the literature, pyrolysis of oil sludge was studied by coupling TGA with an on-line FT-IR spectrometer. Non-isothermal experiments were performed using different heating rates, and the kinetics of the process were analyzed by the Friedman, Flynn-Wall-Ozawa, Kissinger-Akahira-Sunose, Starink, and Tang models. Moreover, thermodynamic parameters such as changes in enthalpy ($\Delta H^{\neq}$), Gibbs free energy ($\Delta G^{\neq}$), and entropy ($\Delta S^{\neq}$) were estimated.

2. Materials and methods

2.1. Experimental study

2.1.1. Preparation and characterization of the sludge

The petroleum sludge was obtained from a petroleum refinery located in İzmit, Turkey (TÜPRAŞ-Turkish Petroleum Refineries Co.). Before the experimental runs, the sludge was dried at room temperature and powdered to a particle size less than 0.125 mm. Afterwards, the main characteristics were determined by proximate and ultimate analyses according to the ASTM standards. The proximate and ultimate analyses of oil sludge is given in Table 1 on a 15-days-air-dried basis. Proximate analysis showed that oil sludge has high volatile matter as 53.25 wt% while ultimate analysis revealed the presence of high carbon content as 50.68 wt%. Since precursors with high carbon and hydrogen and low oxygen contents are preferable for pyrolysis processes, it is convenient to say that pyrolysis can be a suitable thermochemical conversion method to recover the hydrocarbon content of the oil sludge.

For a detailed quantitative ash analysis, the residue obtained after burning the oil sludge sample was analyzed using X-ray fluorescence spectroscopy (Rigaku XRF, ZSX). According to the results, Fe_2O_3 is one of the key mineral species in oil sludge which contributes 31.01 wt% of ash as the major inorganic phase (Table 2). The results of XRF analysis also indicated that oil sludge ash was comprised of a number of oxides such as SiO_2, CaO, Na_2O, MgO. It is known that the presence of metal oxide in ash boosted the active site and enhanced the catalytic effect

Table 1
Proximate and ultimate analyses of air-dried oil sludge.

		wt%
Proximate Analysis	Moisture	3.77
	Ash	34.25
	Volatiles	53.25
	Fixed carbon*	8.73
Ultimate Analysis	Carbon	50.68
	Hydrogen	6.95
	Nitrogen	0.92
	Oxygen*	35.96
	Sulfur	5.49

* From difference

Table 2
Ash composition of oil sludge.

Minerals	Composition (wt%)	Elements	Composition (wt%)
Na_2O	2.3552	Na	2.3509
MgO	1.2510	Mg	1.2487
Al_2O_3	10.8625	Al	10.8425
SiO_2	26.1538	Si	26.1055
P_2O_5	0.4991	P	0.4981
SO_3	14.8649	S	15.0221
K_2O	0.9688	K	0.9670
CaO	10.8853	Ca	10.8652
TiO_2	0.4104	Ti	0.4096
V_2O_5	0.4228	V	0.4221
Cr_2O_3	0.0830	Cr	0.0828
MnO	0.2314	Mn	0.2309
Fe_2O_3	31.0118	Fe	30.9546

during pyrolysis process by affecting cracking and decarboxylation reactions [36].

Fourier Transform Infrared Spectroscopy (FT-IR) analysis of oil sludge was performed using an FT-IR spectrometer (Bruker Tensor 27) to identify structural groups in the range of mid-IR range (4000–400 cm^{-1}) by using KBr pellet technique. In this method, oil sludge sample was mixed with dried KBr in the weight percentage of 1% to prepare pellets for FT-IR analysis. Fig. 1. shows the FT-IR spectrum of oil sludge that includes various surface functional groups. Peaks between 3500 cm^{-1} and 3400 cm^{-1} indicated –OH groups due to the presence of alcohols, phenolics, or carboxylic acids. Aliphatic hydrocarbons showed the main region of strong absorption band between 2800 and 3000 cm^{-1} because of symmetrical and asymmetrical C–H vibrations. Peaks between 1600 and 1650 cm^{-1} were assigned to olefinic C═C vibrations found in aromatic structures. Moreover, peaks between a wavenumber range of 1400–1500 cm^{-1} were caused by C—H bonds in alkane structures and the C-O vibrations resulted in a strong peak around 900–1100 cm^{-1}.

2.1.2. Thermoanalytical measurements

The dried oil sludge samples were subjected to simultaneous TGA/FT-IR analysis. The samples for the non-isothermal pyrolysis experiment were heated from room temperature to 1000 °C in N_2 atmosphere with a flow rate of 20 $ml.min^{-1}$, at heating rates of 5, 10, 20, and 40 °C. min^{-1}. Before each thermochemical conversion analysis, a blank experiment was performed to gain the baselines in order to eliminate the systematic errors of the instrument. A sample of approximately 10 mg was placed within an alumina pan and weight loss, together with other process variables such as time and temperature were monitored during dynamic measurements. During pyrolysis, evolved gases were swept through the capillary transfer lines which were connected to FT-IR spectrometer. To avoid plugging, the transfer line and FT-IR cell were maintained at 225 °C and 250 °C, respectively. FT-IR spectra were recorded from 4000 to 400 cm^{-1} using OMNIC software. To ensure the accuracy of the experimental results, all the experiments were conducted at least twice and average values were used in kinetic analysis.

2.2. Kinetic and thermodynamic analysis

Non-isothermal kinetic analysis was performed using sample weight loss data recorded during pyrolytic degradation. In general, non-isothermal approaches are preferred for pyrolysis experiments since isothermal experiments are imprecise in accounting for the uncertainties of possible chemical reactions during the heating period [37]. During thermal analysis, fractional conversion (α) and pyrolysis reactivity index (R_p) can be expressed by Eq. (1) and Eq. (2), respectively.

$$\alpha = \frac{w_o - w_t}{w_o - w_f} \tag{1}$$

$$R_p = \frac{1}{w_o}\left(\frac{dw}{dt}\right)_{max} \tag{2}$$

In the equations, w_o is the initial weight of the sample (mg), w_t is the instantaneous sample weight (mg) at time t or temperature T, w_f is the final weight of the sample (mg), and $(dw/dt)_{max}$ is the maximum decomposition rate. Char yield (CY), at the end of the main pyrolysis zone, was calculated by the following relationship:

$$CY(\%) = \frac{w_f}{w_0} x100 \tag{3}$$

It is well known that the basic rate equation of the solid-state thermal conversion process assumes that the conversion rate is proportional to the concentration of reactant and dependent on temperature. At a linear temperature heating rate (β); two different independent functions, namely temperature function (k(T)) and fractional conversion function (f(α)); are often used to define the kinetic expression as given in the following equation:

$$\frac{d\alpha}{dt} = \beta\frac{d\alpha}{dT} = k(T)f(\alpha) \tag{4}$$

The temperature dependency of the rate constant, k, is described by the Arrhenius equation [$k = Aexp(-E_a/RT)$] where E_a is the activation energy, A is the pre-exponential factor, and R is the gas constant. Hence, the reaction rate can be given in the form:

$$\beta\frac{d\alpha}{dT} = Aexp\left(-\frac{E_a}{RT}\right)f(\alpha) \tag{5}$$

where f(α) is the conversion function. Eq. (5) can also be integrated into;

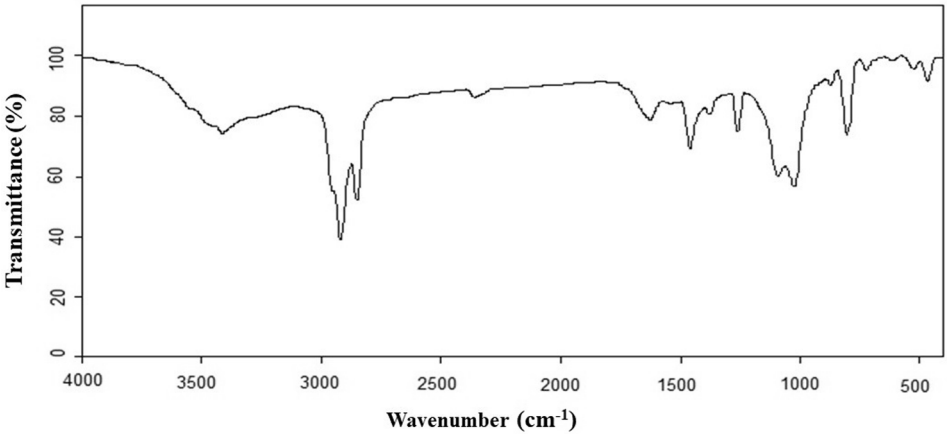

Fig. 1. FT-IR spectrum of oil sludge.

$$\int_0^{\alpha} \frac{d\alpha}{f(\alpha)} = g(\alpha) = \frac{A}{\beta}\int_{To}^{T} exp\left(-\frac{E_a}{RT}\right)dT \equiv \frac{AE_a}{\beta R}p(u) \quad (6)$$

where g(α) and p(u) are known as the integrated form of fractional conversion function, and temperature integral, respectively. Since p(u) has no analytical solution, it can be given by some approximations based on the kinetic methods applied. The above equations can be processed in two ways as model-free and model-fitting methods for the calculation of kinetic parameters. In the model-free approach; knowledge of reaction model f(α) is not required while it is assumed in the case of model-fitting methods. It is accepted that widely-used *iso*-conversional methods are reliable to extract trustworthy and consistent kinetic information from both isothermal and non-isothermal data [38]. The basis of the *iso*-conversional approach is that the rate of decomposition is calculated by the current sample temperature at a certain point of conversion. Moreover, heating rate and temperature changes are considered ineffective to the reaction mechanism [39]. In the scope of this study Friedman [40] and Flynn-Wall-Ozawa [41,42], KAS [43,44], Starink [45], and Tang [46].models were employed without assuming any reaction route in a model-free approach to analyze kinetic characteristics of petroleum sludge. After the determination of activation energy, thermodynamic parameters as the changes in enthalpy, Gibbs free energy, and entropy can be estimated using the activated complex (transition state) theory. Accordingly, the transition-state entropy change, $\Delta S^{\neq}$, is related to the pre-exponential factor:

$$\Delta S^{\neq} = Rln\frac{Ah}{e\chi k_B T_p} \quad (7)$$

where: e = 2.7183 is the Neper number; $\chi$is the transmission factor, which is considered as unity for mononuclear reactions; k_B is Boltzmann constant (1.381×10^{-23} J.K^{-1}); h is the Plank constant (6.626×10^{-34} J.s) and T_p is the average peak temperature observed from the dTG curves at different heating rates. In general, transition state theory is developed for monomolecular and bimolecular reactions taking place in the gas phase. On the other hand, several authors used this approach for solid-based reactions [47–49]. Due to the complex scheme of radical reactions during tar pyrolysis, the activation entropy calculated by the transition state theory must be considered as an apparent value that is convenient only for analyzing the heterogeneity of the tar [50]. The usage of this approach is acceptable after considering the specific surface area of the solid (S_{BET}), the length of the molecular unit considered in the decomposition (L), and the true density of the solid (ρ) as given in Eq. (8) [50]. In order to apply Eq.8, the BET surface area of the oil sludge was determined by N_2 adsorption at 77 K with a surface area analyzer (Quantachrome Autosorb) and density of the sludge was determined by gas pycnometer (Quantachrome 1200e), using helium gas at a pressure of 20 psia for the calculation of thermodynamic parameters.

$$\Delta S^{\neq} = Rln\frac{Ah}{S_{BET}L\rho e\chi k_B T_p} \quad (8)$$

After calculation of $\Delta S^{\neq}$, the changes of the enthalpy ($\Delta H^{\neq}$), and Gibbs free energy ($\Delta G^{\neq}$) can be then calculated via Eqs. (9) and (10).

$$\Delta H^{\neq} = E_a - RT_p \quad (9)$$

$$\Delta G^{\neq} = \Delta H^{\neq} - T_p\Delta S^{\neq} \quad (10)$$

3. Results and discussion

3.1. Thermogravimetric analysis of oil sludge

TG curves were used to interpret the mass loss behavior during thermal degradation, while dTG curves were used to determine the maximum temperature of pyrolytic degradation together with the onset and offset temperatures of the main active pyrolysis region. The TG and dTG curves at four different heating rates are illustrated in Fig. 2 to show the pyrolysis behavior of oil sludge. Furthermore, Table 3 summarizes the characteristic temperatures related to pyrolytic degradation. A small weight loss before 120 °C may be attributed to the loss of moisture and low molecular weight hydrocarbons which is consistent with proximate analysis. For the heating rate of 5 °C.min^{-1}, the weight-loss of the main decomposition was from 178.5 to 493.9 °C, yielding 49.97 wt% char. As seen from the thermographs, this second stage yielded a large amount of volatiles. When the temperature reached 432.2 °C, the weight loss rate reached its peak value which indicated the maximum rate of weight loss. The main mass slopes of the TG curves and the most dominant peaks of dTG thermograms for all heating rates (5 to 40 °C.min^{-1}) were observed between 178.5 and 535.8 °C, which were due to the thermal decomposition of oil sludge in the active pyrolysis region. Thermal cracking of organics and devolatilization of fragments generated from the cleavage of covalent bonds occurred in this intensive mass loss region. Fragmentations in the active pyrolysis region were acceptable in terms of the weight loss trend and the multi-stage nature of the pyrolytic reactions. It is notable that pyrolysis reactivity was gradually increased from 0.16 to 1.35 s^{-1} while the heating rate varied from 5 to 40 °C.min^{-1}. The weight-loss stage after this main zone was the carbonization stage where the TG and dTG curves were almost decelerated and the solid residue from the second stage was carbonized. This final stage of pyrolytic decomposition was accompanied by depolymerization and repolymerization of macromolecules that existed in the structure of the sludge. The further calculations for kinetics and thermodynamics were based on the active pyrolysis zone whose characteristic temperatures are given in Table 3.

The effect of increasing heating rate on the decomposition resulted in an increment of a lateral shift in the temperature of the maximum degradation peak. This occurrence is due to the combined effect of heat transfer at different heating rates and the heat conductive property of the sludge which is used in the pyrolysis process [51]. As the heating rate was increased from 5 to 40 °C.min^{-1}, the specific decomposition temperature increased, which was related to the different heat-transfer rates that also; affected the thermal decomposition kinetics. The variation in the mass loss rate might be attributed to the considerable difference of temperature between the surface and the interior sections of the particle at a high heating rate [52]. As illustrated in the figure, increases in the heating rate had no effect on the decomposition mechanism since the shape of the peaks remained nearly the same while the pyrolytic decomposition rate changed.

3.2. Estimation of activation energy

Iso-conversional methods are the fastest approaches yielding satisfactory accurate results to obtain activation energy without requiring prior knowledge of the conversion function. Extraction of the activation energies of thermally activated reactions from non-isothermal TGA data with the help of *iso*-conversional methods is considered as some of the most reliable techniques [53]. However, the *iso*-conversional approach gives a systematic error in the calculations when the activation energy strongly varies with the conversion degree. This error may be eliminated by performing multi-stage kinetic analysis using different approaches that properly account for the changes in the activation energy. For this purpose, a multi-peak fitting method was used to separate and analyze the overlapping peaks for oil sludge pyrolysis during the active pyrolysis stage. According to TG and dTG curves, oil sludge pyrolysis was assumed to involve a multi-step decomposition mechanism due to the complex reaction scheme. Therefore, a peak deconvolution approach was used to analyze the main thermal degradation zone and an asymmetric double sigmoidal (Asym2sig) function was implemented to the experimental TGA data. The experimental curves for all heating rates were simplified by this method and the two sub-stage curves for pseudo-reactions or pseudo-degradation zones occurring during oil sludge pyrolysis were achieved.

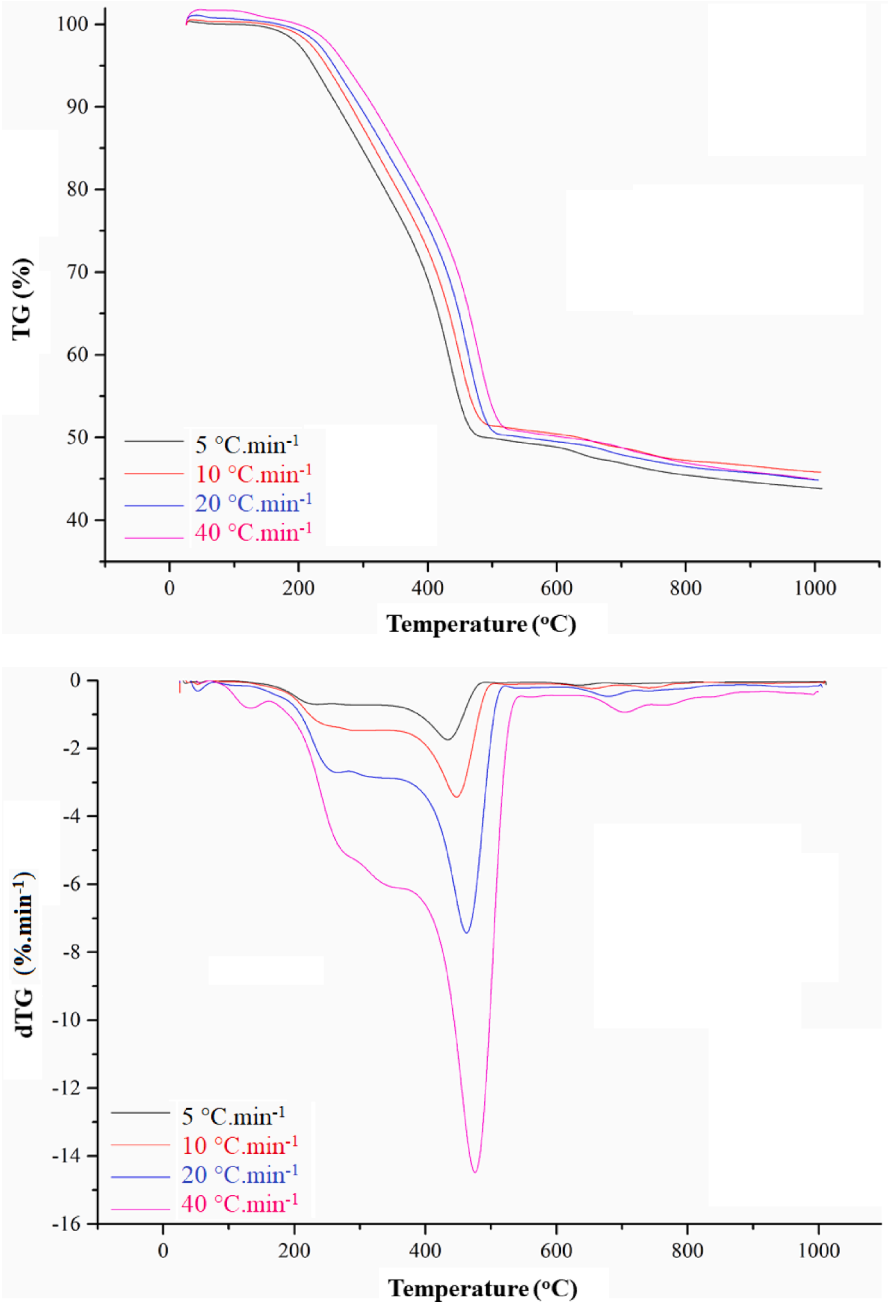

Fig. 2. TG and dTG curves of oil sludge at the different heating rates.

Table 3
Thermal decomposition characteristics of oil sludge at active pyrolysis region.

β (°C.min^{-1})	T_i* (°C)	T_{max}** (°C)	T_f*** (°C)	CY (wt. %)	R_p**** (s^{-1})
5	178.5	434.2	493.9	49.97	0.16
10	180.3	447.6	504.5	51.38	0.32
20	182.1	462.8	514.9	50.33	0.69
40	184.9	475.7	534.8	50.42	1.35

* T_i: Temperature at which the decomposition is started.
** T_{max}: Temperature at which the highest decomposition rate is observed.
*** T_f: Temperature at which the decomposition is completed.
**** R_p: Pyrolysis reactivity index.

The results of the curve fitting given in Fig. 3 can be explained by the existence of two decomposition reaction zones during active pyrolysis of oil sludge. The two sub-stages were called Fit Peak 1 and Fit Peak 2. The fitting quality of these two peaks with the experimental data was evaluated with statistical parameters. The cumulative curves were highly correlated with the experimental data for all heating rates. The deconvolution parameters provided a satisfactory adjustment, with adjusted r-square (Adj. R^2) values between 0.98892 and 0.99241. Moreover, small reduced chi-square values between 0.00129 and 0.21869 indicated excellence of the cumulative fit. Based on this data extraction, the activation energies of each pseudo reaction zones were examined using *iso*-conversional kinetic methods by changing the conversion degree from 0.1 to 0.9 with increments of 0.1. The conversion degree ranges under 0.1 and above 0.9 were not considered during the calculations, since equipment sensitivity may lead to data deviations with low decomposition rates. The activation energies calculated with different models for each conversion degree are summarized in Table 4 for comparison. Moreover, the linear plots of the Friedman model are shown in Fig. 4, and the activation energies obtained at different

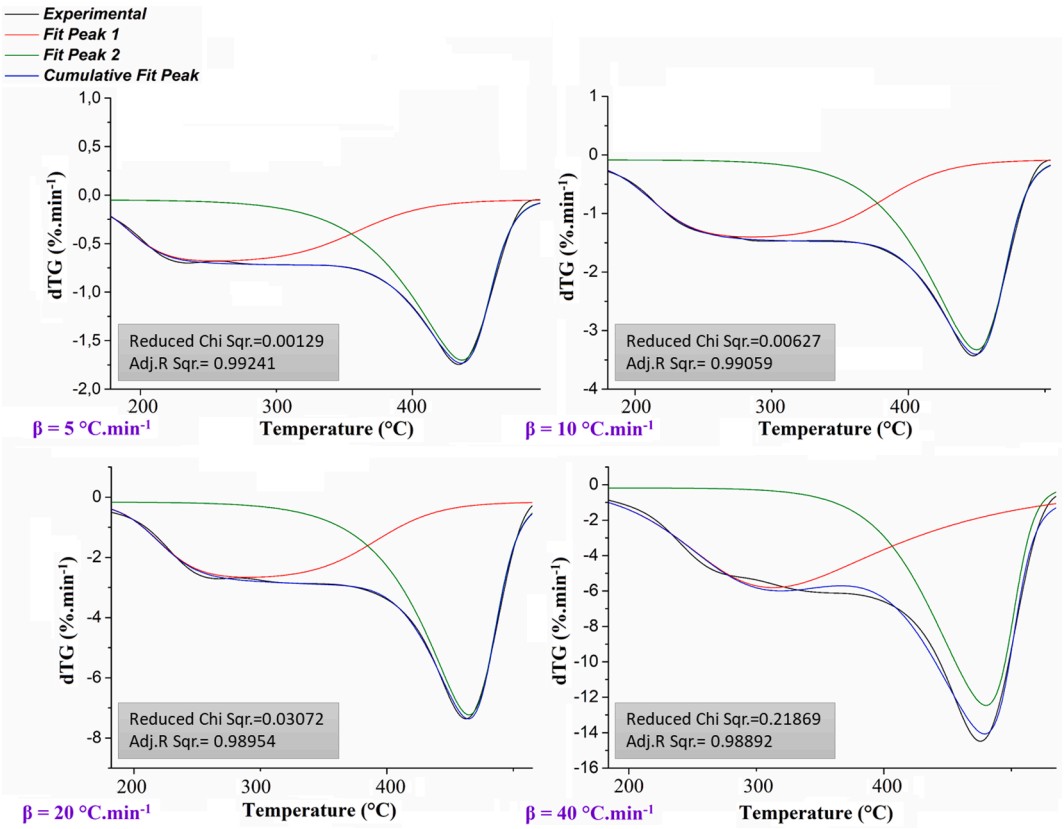

Fig. 3. Deconvoluted dTG curves for oil sludge pyrolysis at the different heating rates.

Table 4
Activation energies (kJ.mol^{-1}) with respect to conversion degree for pyrolysis of oil sludge.

	α	Friedman		FWO		KAS		Starink		Tang	
		E_a	R^2	E_a	R^2	E_a	R^2	E_a	R^2	E_a	R^2
1st stage	0.1	103.709	0.9992	118.127	0.9988	115.856	0.9987	116.265	0.9987	116.128	0.9987
	0.2	102.886	0.9927	107.363	0.9960	104.174	0.9951	104.660	0.9952	104.480	0.9952
	0.3	109.279	0.9938	109.141	0.9942	105.754	0.9931	106.267	0.9932	106.074	0.9932
	0.4	114.201	0.9917	112.697	0.9909	109.221	0.9892	109.754	0.9894	109.553	0.9893
	0.5	116.088	0.9919	115.906	0.9919	112.322	0.9904	112.869	0.9905	112.666	0.9905
	0.6	113.860	0.9931	117.115	0.9952	113.320	0.9943	113.888	0.9944	113.670	0.9944
	0.7	107.300	0.9978	115.432	0.9963	111.233	0.9955	111.842	0.9956	111.603	0.9956
	0.8	98.737	0.9900	111.559	0.9998	106.818	0.9997	107.468	0.9997	107.212	0.9997
	0.9	91.254	0.9895	107.134	0.9956	101.722	0.9948	102.440	0.9949	102.147	0.9948
$\bar{x}$		**106.4**	**0.9933**	**112.7**	**0.9954**	**108.9**	**0.9945**	**109.5**	**0.9950**	**109.3**	**0.9946**
SD		7.653		3.946		4.388		4.343		4.366	
2nd stage	0.1	194.115	0.9953	192.716	0.9945	191.704	0.9939	192.099	0.9940	192.008	0.9939
	0.2	197.075	0.9956	192.336	0.9941	190.981	0.9934	191.403	0.9935	191.294	0.9935
	0.3	201.972	0.9978	196.786	0.9959	195.429	0.9955	195.868	0.9955	195.752	0.9955
	0.4	204.907	0.9992	200.168	0.9974	198.804	0.9972	199.248	0.9972	199.139	0.9972
	0.5	206.886	0.9999	202.745	0.9986	201.373	0.9985	201.816	0.9985	201.704	0.9985
	0.6	208.789	0.9998	204.847	0.9994	203.444	0.9993	203.895	0.9993	203.780	0.9993
	0.7	211.641	0.9996	206.902	0.9998	205.481	0.9998	205.941	0.9998	205.822	0.9998
	0.8	216.738	0.9996	209.581	1.0000	208.166	0.9999	208.624	0.9999	208.512	0.9999
	0.9	226.681	0.9997	214.433	0.9999	213.121	0.9999	213.578	0.9999	213.460	0.9999
$\bar{x}$		**207.6**	**0.9985**	**202.3**	**0.9977**	**200.9**	**0.9975**	**201.4**	**0.9980**	**201.3**	**0.9975**
SD		9.413		7.104		7.048		7.065		7.060	

$\bar{x}$**:** Average value.
SD: Standard deviation.

conversions using different *iso*-conversional methods are compared for a better illustration in the same figure. In general, a reaction with lower activation energy requires a lesser amount of energy to disintegrate the chemical bonds between atoms, and consequently, the related reaction can be processed easier. On the contrary, relatively high activation energy implies a higher temperature requirement to decompose the structure [54,55]. Approximately the same values for the activation energy at different conversion degrees are attributed to similar kinetic behavior, probably the same reaction mechanism. On the other hand, higher deviations and fluctuations in the values of the activation energy at different conversion degrees suggest that there are distinct mechanisms for the overall conversion process [54,55]. According to the

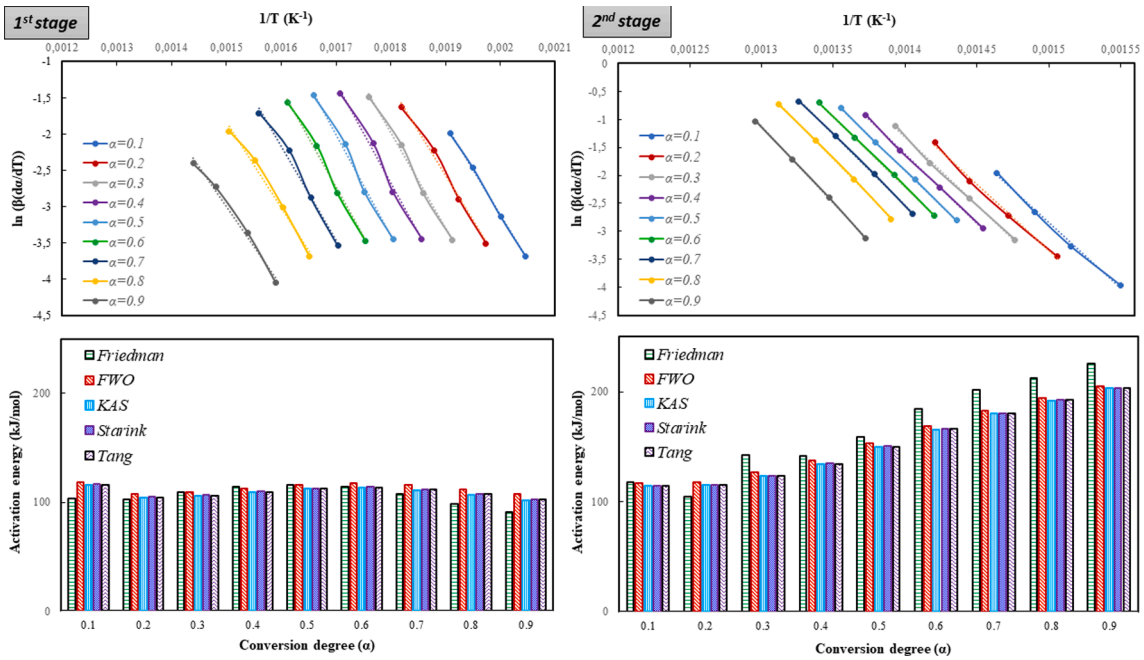

Fig. 4. Friedman plots for calculation of activation energy and activation energy obtained at different conversions using different *iso*-conversional methods for two degradation stages.

activation energy calculations in this study, a complex reaction scheme with parallel and competitive reactions occurred during pyrolysis of oil sludge. It was observed that the activation energies of the first stage varied between 116.1 and 91.3 kJ.mol^{-1} with an average value of 106.4 kJ mol^{-1} according to the Friedman method (Table 4). The activation energies of the first pyrolytic degradation seemed to decrease with the increase in conversion, especially after a certain conversion degree of 0.5 for Friedman and 0.6 for the other models. The activation energy at the nearly mid-conversion degree was the highest in comparison to the values at other conversion degrees, which reflected that some highly endothermic reactions took place at this stage. It is inevitable to observe from the Friedman plots that, the lines were not in parallel, and the variations of their slopes indicated the progress of the reactions during the first degradation zone. The non-parallelism of the Friedman plots pointed out the high probability of changing kinetic parameters during the pyrolysis of oil sludge [56]. The fluctuations of the activation energy with the conversion degree were probably due to the extent of the reaction process, particularly the change in the structure of oil sludge as the temperature increased. The average the activation energies during the first degradation zone calculated from the FWO, KAS, Starink, and Tang models were 112.7, 108.9, 109.5, and 109.3 kJ.mol^{-1}, respectively.

The Friedman plots showed a non-parallel order with each other during the second sub-stage of pyrolytic degradation, which promoted the idea that the kinetic parameters in the aforementioned region might not be stable. For the second stage of the pyrolytic decomposition, activation energy values tend to increase with conversion degree which means that the energy required for the final stages of the pyrolysis was higher than that of initial reactions. This change could be due to the more complex reactions for the remaining carbonaceous fraction of the sludge. The highest activation energy was obtained by the Friedman method as 226.7 kJ.mol^{-1} at a conversion degree of 0.9 for the second stage. The activation energies of the second stage were also found to be highly dependent on the conversion degree. On average, the best fitting with the experimental data was obtained by the Friedman model for the second stage and the small deviations in the models were attributable to the approximations. The average activation energies of the oil sludge calculated from the Friedman, FWO, KAS, Starink, and Tang models were 207.6, 202.3, 200.9, 201.4, and 201.3 kJ.mol^{-1}, respectively during the second zone. The average activation energy of the second zone was apparently higher than that of the first zone which indicates a higher amount of energy requirement at higher temperatures and the second pseudo-reaction zone is complicated than the first one. Throughout the study, the results obtained by various *iso*-conversional methods were in good agreement with each other, and the variation trend of the activation energy was comparable. Furthermore, the average regression coefficients, which were between 0.9933 and 0.9985, validated the reliability of the calculations and confirmed the predictive power of the applied models (Table 4).

The activation energies belonging to pyrolysis of oil sludge samples in the literature are summarized in Table 5 and experimental conditions are highlighted in the tabulated results. The subtle point to consider is that every sample has its decomposition characteristics owing to its chemical composition and origin. Samples from the crude oil storage tank, tanker cleaning, oil sludge reduction station, and API separator were previously analyzed by several authors [16,32,35,57,58]. Moreover, Choudhury et al. used a complex oily sludge that consists of sludge from an oil storage tank, biological sludge, the dissolved air flotation scum sludge, API separator sludge, and the chemical sludge [59]. According to the findings of previous researchers, differences in the source may lead to different degradation behaviors of sludge components and their interactions. Therefore, it is convenient to say that the activation energy of the oil sludge pyrolysis process is highly susceptible to the characteristics and origin of the sample together with experimental and computational methods that were used.

3.3. Determination of Pre-exponential factor and thermodynamic parameters

The pre-exponential factor represents the number of collisions per unit time that is required to obtain the proper orientation for the reaction to take place. Since it elucidates the reaction chemistry, the determination of the pre-exponential factor is crucial for the optimization of pyrolysis processes. Therefore, the pre-exponential factor at each conversion level was calculated using the activation energies obtained from the Friedman model, and the results are given in Table 6. Low pre-

Table 5
Activation energies of various oil sludge samples.

Origin of the sludge	β (°C.min^{-1})	α	T (°C)	Kinetic method	E_a (kJ.mol^{-1})	Reference
Oil contaminated soil-China	20	0.20–0.80	298–805	FWO	25.5–32.0	Qu et al. (2019)
				KAS	20.8–26.3	
	60		306–872	FWO	38.0–69.9	
				KAS	30.6–62.6	
	100		323–879	FWO	98.9–118.4	
				KAS	92.2–111.7	
Sludge of crude oil storage tank-Taiwan	5.2–21.8	0.10–0.80	Appx. 177–527	One-reaction model	78.2	Shie et al. (2020)
				Two-reaction model	74.33	
					123.4	
				Three-reaction model	69.9	
					93.8	
					123.2	
Sludge of tanker cleaning- China	10.0–50.0	0.06–0.94	Appx 400–800	Vyazovkin model (Two-reaction stages)	59.6	Liu et al. (2009)
					102.0	
Oil sludge reduction station-China	10.0–40.0	0.25–0.95	246–554	Friedman model (Two-reaction stages)	84.7	Cheng et al. (2018)
					145.2	
				Starink model (Two-reaction stages)	82.4	
					147.8	
API separator sludge-Thailand	5.0	0.00–1.00	Appx. 230–440	Coats&Redfern model (Two-reaction stages)	39.84	Punnaruttanakun et al. (2003)
					125.1	
	10.0			Coats&Redfern model (Two-reaction stages)	39.4	
					128.3	
	20.0			Coats&Redfern model (Two-reaction stages)	37.2	
					160.1	
Mixed refinery sludge -India	5–20	0.05–0.95	100–500	KAS	74.8–657.0	Choudhury et al. (2007)
				Flynn–Wall	83.1–610.0	
				Friedman	39.0–473.0	
				One-reaction model	88.3	
				Two-reaction model	64.0	
					112.0	
Sludge of crude oil storage tank-Turkey	5–40	0.10–0.90	178–535	Friedman (Two-reaction stages)	103.7–91.2	This study
					194.1–226.7	
				FWO (Two-reaction stages)	118.1–107.1	
					192.7–214.4	
				KAS (Two-reaction stages)	115.9–101.7	
					191.7–213.1	
				Starink (Two-reaction stages)	116.3–102.4	
					192.1–213.6	
				Tang (Two-reaction stages)	116.1–102.2	
					192.0–213.5	

exponential factors, which are below 10^9 s^{-1}, imply a system with less reactivity where surface reactions are dominant. However, if the reactions are not dependent on the surface area, the low pre-exponential factor may indicate a closed complex. Otherwise, high pre-exponential factors, which are greater than 10^9 s^{-1}, represent a highly reactive system with a simple complex. In particular, the activated complex is probably hindered in rotation in comparison to the initial reagent when the pre-exponential factors are between 10^{10} and 10^{11} s^{-1} [60,61]. In this study, the pre-exponential factors showed variation in a wide range between 1.20×10^5 and 3.20×10^7 s^{-1} at different conversion degrees for the first active pyrolysis zone. At the initiation of the pyrolytic degradation process, an increase in the pre-exponential factor was observed from the conversion degree of 0.1 to 0.5. Then, the values tended to decrease till the end of the first zone. This may be attributed to the heterogeneous composition of the oil sludge and the complex reactions. On the other hand, the intensity of collisions tended to increase steadily during the second sub-zone of active pyrolysis. The highest value of the pre-exponential factor was observed as 1.24×10^{13} s^{-1} at the conversion degree of 0.9 while the mean value was 1.91×10^{12} s^{-1}. A comparison between two sub-zones indicated that surface reactions dominated the initial degradation stage whereas collision intensity increased during the second stage with simple complex formation. Overall, this wide range of variation in the pre-exponential factor was due to the complex organic and inorganic nature of the oil sludge and the involvement of several parallel and consecutive reactions during the pyrolytic decomposition process.

For most chemical reactions, the effect of an alteration in the activation energy is presumed to decline the reaction rate at a particular temperature. This is partially or entirely offset by a compensatory increase in the pre-exponential factor, which is called the kinetic compensation effect [62]. To put it into other words, when a change of the activation energy is noticed, there is a shift in the numerical values of the pre-exponential factor. The validity of the compensation effect is also considered as a statistical deviation, due to the necessity of extrapolation to calculate the pre-exponential factor [63,64]. The compensation effect evaluation for oil sludge pyrolysis with a linear relationship between the activation energy and the natural logarithmic form of the pre-exponential factor was also confirmed by a correlation coefficient of unity as shown in Fig. 5. Accordingly, the linear plots obtained by the compensation effect which describes a linear relationship between the activation energy and the pre-exponential factor for the first and second stages were given by Eqs. (11) and (12).

$$\ln A = 0.2249E_a\text{-}8.8255 \text{ for stage 1} \quad (11)$$

$$\ln A = 0.1711E_a\text{-}8.6378 \text{ for stage 2} \quad (12)$$

Based upon the calculated pre-exponential factors at each conversion degree, enthalpy, entropy, and Gibbs free energy changes were calculated and are presented in Table 6 to comment on the nature of the pyrolytic degradation process of the oil sludge. Enthalpy is known to be a significant thermodynamic parameter that shows the energy requirement of a system. High enthalpy changes during the process establish a high energy requirement [65]. A small difference between the activation energy and the variation of enthalpy indicates the probability of the

Table 6
Pre-exponential factors and thermodynamic parameters of oil sludge pyrolysis.

	α	A (s^{-1})	$\Delta H^{\neq}$ (kJ.mol^{-1})	$\Delta G^{\neq}$ (kJ.mol^{-1})	$\Delta S^{\neq}$ (J.mol^{-1}. K^{-1})
1st stage	**0.1**	1.99×10^{6}	99.07	155.37	−100.86
	0.2	1.65×10^{6}	98.24	155.41	−102.40
	0.3	6.94×10^{6}	104.64	155.13	−90.45
	0.4	2.09×10^{7}	109.56	154.93	−81.28
	0.5	3.20×10^{7}	111.45	154.86	−77.76
	0.6	1.94×10^{7}	109.22	154.94	−81.91
	0.7	4.45×10^{6}	102.66	155.21	−94.15
	0.8	6.48×10^{5}	94.10	155.59	−110.17
	0.9	1.20×10^{5}	86.61	155.95	−124.22
	$\bar{x}$	$\mathbf{9.79 \times 10^{6}}$	**101.7**	**155.3**	**−95.9**
2nd stage	**0.1**	4.70×10^{10}	188.03	200.56	−17.12
	0.2	7.81×10^{10}	190.99	200.43	−12.90
	0.3	1.81×10^{11}	195.89	200.23	−5.93
	0.4	2.99×10^{11}	198.82	200.10	−1.75
	0.5	4.19×10^{11}	200.80	200.02	1.07
	0.6	5.81×10^{11}	202.71	199.94	3.78
	0.7	9.46×10^{11}	205.56	199.83	7.83
	0.8	2.26×10^{12}	210.66	199.62	15.08
	0.9	1.24×10^{13}	220.60	199.23	29.20
	$\bar{x}$	$\mathbf{1.91 \times 10^{12}}$	**201.6**	**200.0**	**2.1**

pyrolysis reaction to occur. Furthermore, positive values of enthalpy change inform the endothermal character of pyrolysis that requires an external energy source to provide a high energy level, capable of promoting reagents to their transition state [66]. If this enthalpy change is small, the formation of an activated complex is favored due to the low potential energy barrier.

For the oil sludge pyrolysis, the variation of enthalpy change followed a similar trend to the activation energy for the two decomposition stages. The enthalpy changes depicted a rising trend until a conversion degree of 0.5 for the first stage which occurred at lower temperatures. The lowest value of the enthalpy change was observed at a conversion degree of 0.9 as 86.6 kJ.mol^{-1} for this stage. On the other hand, enthalpy change was continuously increased from 188.0 to 220.6 kJ.mol^{-1} when the conversion degree was increased from 0.1 to 0.9 for the second stage. The changes in the enthalpy were estimated to be 101.7 and 201.6 kJ.mol^{-1} on average for the first and second stage, respectively, which indicated the fragmentation of the recalcitrant structure of the sludge into liquid, solid and gaseous products.

Gibbs free energy represents the increase in the total energy of the reaction during the formation of the activated complex [67]. Positive values of Gibbs free energy change at each conversion degree of the pyrolytic degradation of the oil sludge implied that the process had a non–spontaneous nature, and it required an external heat supply to occur. The change in the Gibbs free energy was found between 154.9 and 200.6 kJ.mol^{-1} during the overall process. The highest value of the Gibbs free energy change at a conversion degree of 0.1 of the second stage denoted a lower favorability for pyrolytic conversion at the initiation of the second temperature zone. The mean Gibbs free energy changes were calculated as 155.3 and 200.0 kJ.mol^{-1} for the first and second stages, respectively.

Another thermodynamic parameter considered in this study was entropy change that is known to manifest the degree of disorder of the pyrolytic decomposition reactions. A negative entropy change suggests that the reaction system moves from a disordered state to an ordered one, which is of great importance to converting oil sludge into fuels and chemicals. A low entropy change means the material just passes through some physical and chemical changes, bringing it to a state near to its thermodynamic equilibrium [67]. The entropy change of oil sludge pyrolysis was negative during the first stage of active pyrolysis, while it was steadily decreasing after a conversion degree of 0.5. The negative values of the entropy change in the first stage confirmed that the intermediate states in the decomposition process possessed a higher

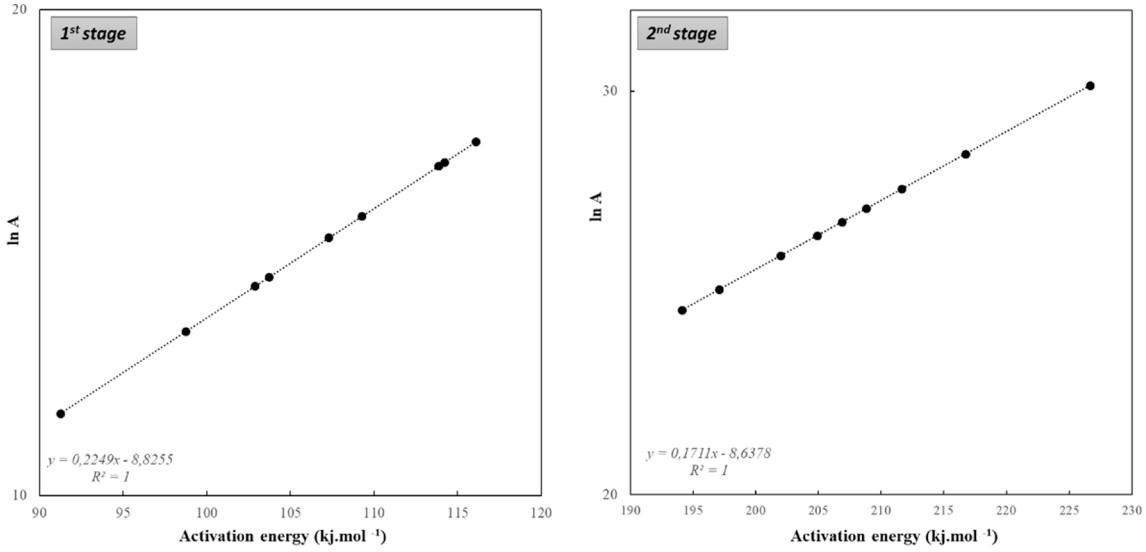

Fig. 5. Compensation effect plot (ln(A) versus E_a) for oil sludge pyrolysis.

degree of arrangement than the initial substance that existed with an average entropy change of −95.91 J.mol^{-1}.K^{-1}. Therefore, the average entropy change during the first degradation stage was negative, which showed that the orderliness increased and the degree of reaction progress was more difficult to spontaneously accelerate, so it required additional energy injection into the reaction system during lower temperatures of the active pyrolysis [68]. Negative values of entropy change also pointed out that the activated complex can be classified by a much-developed degree of arrangement during the first stage [69]. On the other hand, high entropy changes represent high reactivity and less time to form activated complex [70]. The values of entropy change were found to be between −17.12 and 29.20 J.mol^{-1}.K^{-1} with an average value of 2.1 J.mol^{-1}.K^{-1}. Notably, entropy change turned positive after a conversion degree of 0.4 for the second stage of the active pyrolysis that occurred at higher temperatures. A positive entropy change denotes the increase in the disorder of the system as the reaction proceeds [71]. Maxima in the entropy change value at 0.9 conversion degree of the second stage indicates the highest reactivity of the system at this point of conversion due to subsequent char gasification after active pyrolysis.

3.4. Evolved gas analysis by simultaneous TGA/FT-IR

TGA/FT-IR analysis was employed to determine the distribution of volatiles according to their functional groups against temperature to evaluate the decomposition characteristics. Fig. 6 shows the simultaneous FT-IR spectra obtained during pyrolysis at two different heating

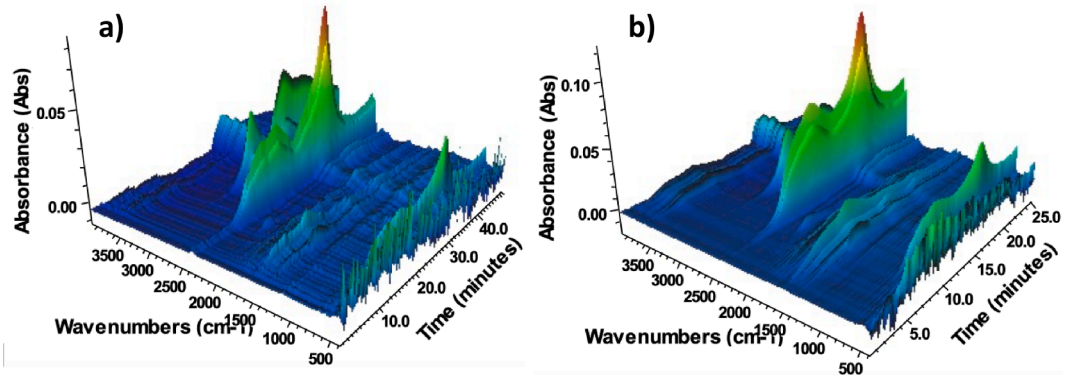

Fig. 6. 3D FT-IR spectra of oil sludge pyrolysis (Heating rates (a) 20 and (b) 40 °C.min^{-1}).

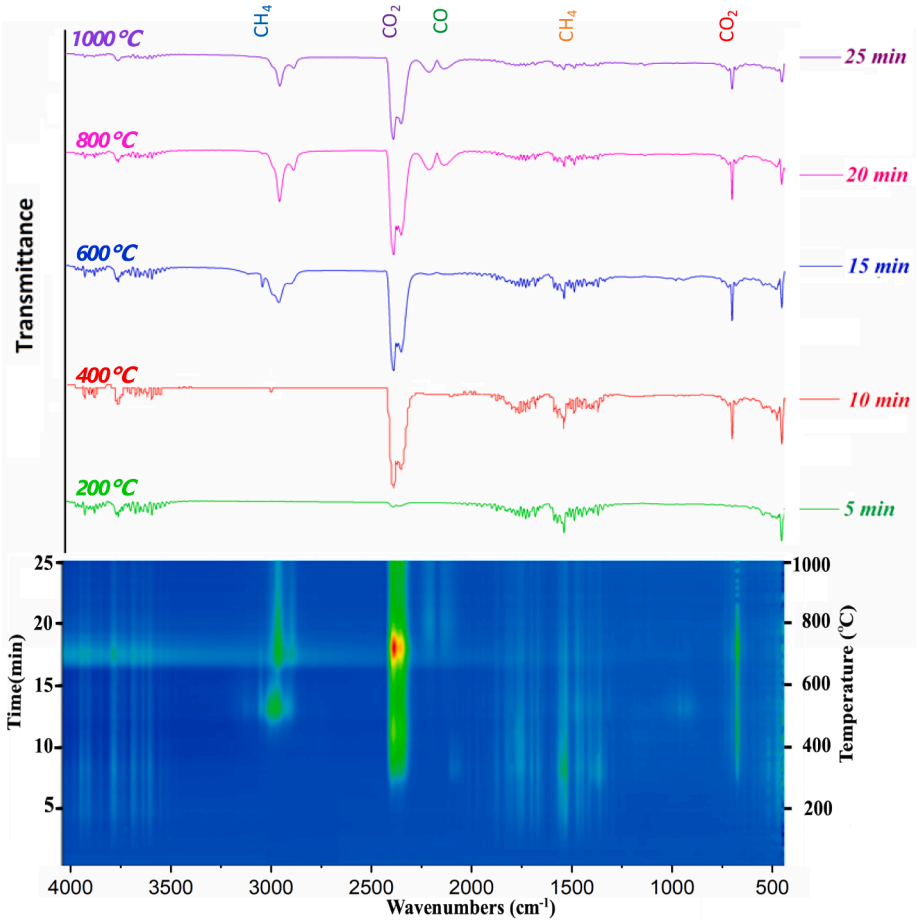

Fig. 7. Changes in the instantaneous spectra of the released gasses during pyrolysis (β = 40 °C.min^{1}).

rates, and the plots represent the variation of absorbance with respect to time and wavenumber. Additionally, the instantaneous FT-IR spectra were recorded at different degradation times and hence different temperatures to illustrate the evolution of gases at the main stages of conversion (Fig. 7). As can be seen, the gas evolution profiles are close to each other, revealing the similar decomposition behavior at heating rates of 20 °C.min^{-1} and 40 °C.min^{-1}. The 3D spectrum of the oil sludge exhibited a variety of absorption bands corresponding to different functional groups and their overlapping peaks. However, only a group of substances can be decisive due to the complexity of the evolved gases generated during the pyrolysis process and the limitations of FT-IR analysis [72–74]. In this study, the absorption bands with high intensities were evaluated, although there were smaller peaks for other vibrations such as –OH (assigned to the presence of water, alcohol, or phenolics) and N–H (assigned to amines) due to the presence of remarkable amounts of O and N in the raw material.

The two notable bands at around 2400–2240 cm^{-1} and 730–630 cm^{-1} were ascribed to the release of CO_2. According to the Lambert-Beer law, the absorption intensity of the FT-IR spectrum was correlated with the concentration of the evolved gases during the pyrolytic degradation process. Since the intensities for CO_2 absorption bands were significantly higher than that of the other functional groups, it can be concluded CO_2 was the main gas product of devolatilization reactions. As seen from Figs. 6 and 7 CO_2 was started to be dominated after the initiation of the main degradation zone and attained a peak at about 420 °C (10 min). The highest intensity of the CO_2 peak was observed at around 700 °C (17 min) which was higher than the maximum degradation rate temperature (Table 3). The time lag between TGA and FT-IR and the high heating rate (40 °C.min^{-1}) were the reasons for this difference in the recorded temperatures. The generation of CO_2 continued after the active pyrolysis zone till the end of decomposition, which might be attributed to the further decomposition of the evolved gases by secondary reactions such as cracking and gasification during oil sludge pyrolysis.

During the degradation of oil sludge, the evolution of various hydrocarbon species was noticed from the C–H stretching and bending vibrations at around 3050–2850 cm^{-1} and 1500–1380 cm^{-1}, respectively. The absorption band between 3000 and 2800 was attributed to stretching vibrations of aliphatic C–H groups which represented the presence of multiple organic compounds such as alkanes, alkenes, ketones, aldehydes, alcohols, and other hydrocarbons. However, for the decomposition of organic precursors under an inert atmosphere, the peaks at around 2950 and 2850 cm^{-1} were assigned to CH_4 formation. The demethylation reactions might be attributed to the removal of the aliphatic structure bonded on the aromatic cores of the sludge sample. The C–H stretching vibrations of aromatic structures were detected as a sharp peak around 3010 cm^{-1} at the 15th-minute spectrum (Fig. 7). As the temperature increased, this band was removed from the spectra due to the secondary fragmentation reactions of the volatiles into smaller molecules at higher temperatures. As can be seen from the 2D FT-IR spectrum, C–H bands started at the 12th minute that corresponds to approximately 500 °C and the first peak was completed at 15.5 min. The second CH_4 release was observed after 16.5 min and nearly completed around 19 min. The bands observed at higher temperatures were due to the time lag as described above.

Two bands located between 2250 and 2050 cm^{-1} with a distinct peak at 2190 cm^{-1} representing C–O stretching vibrations indicated the formation of CO along with the CO_2 at the higher temperatures due to char gasification. The initial formation of CO was not seen until the 16th minute (660 °C) where the second group of volatilization reactions occurred from the highest amount of CO_2.

4. Conclusions

This study presented a TGA/FT-IR analysis of the thermochemical conversion of petroleum refinery waste (oil sludge) and the following conclusions were derived:

Based on the TGA data, the decomposition of oil sludge took place over a wide temperature range of 180–505 °C when 10 °C.min^{-1} heating rate was applied. The pyrolysis heating rate influenced the thermal reactivity of the oil sludge.

When different *iso*-conversional methods were used for kinetic analysis, an alteration in the activation energy with conversion degree was noticed, which indicated that the pyrolytic degradation of oil sludge progressed through multi-step and complex reactions. Concerning the determination of kinetic parameters, a two-stage degradation zone was determined using peak deconvolution.

The average activation energy for the first degradation zone during active pyrolysis was calculated to be 106.4 kJ.mol^{-1} from the Friedman model while the second stage had an average activation energy of 207.6 kJ.mol^{-1}. The results implied that the Flynn-Wall-Ozawa, Kissinger-Akahira-Sunose, Starink, and Tang models were also suitable for the determination of kinetic parameters of petroleum sludge pyrolysis and described the process realistically.

According to the thermodynamic analysis, the nature of pyrolytic degradation presented a multi-stage intricate reaction phenomenon in which a series of simultaneous complex reactions occurred in the active pyrolysis zone. The positive enthalpy change (an average of 101.7 and 201.6 kJ.mol^{-1} for the first and second sub-stages, respectively) indicated the endothermicity of the overall decomposition process.

The volatiles evolved during pyrolysis were analyzed simultaneously by FT-IR coupled to TGA to study the main constituents of the gases through their functional groups. The main gases released were detected to be CO_2, CH_4, and CO in the decreasing order of absorbance values.

As a result, the kinetic and thermodynamic information presented in this study can be considered to guide the design and development of oil sludge pyrolysis technologies. Furthermore, evolved gas analysis can be beneficial for describing practical pyrolytic conversion, designing and optimizing the efficient pyrolysis technology for petroleum sludge, especially for refineries.

CRediT authorship contribution statement

Gamzenur Özsin: Software, Validation, Formal analysis, Writing - original draft. **Esin Apaydın-Varol:** Methodology, Project administration, Resources, Writing - review & editing, Supervision. **Murat Kılıç:** Investigation, Resources, Writing - review & editing. **Ayşe E. Pütün:** Conceptualization, Supervision. **Ersan Pütün:** Supervision.

Declaration of Competing Interest

The authors declare that they have no known competing financial interests or personal relationships that could have appeared to influence the work reported in this paper.

Acknowledgments

The authors thank Anadolu University Scientific Research Projects Unit for providing financial support with the Grant No: 1202F030 and TÜPRAŞ (Turkish Petroleum Refineries Co.) İzmit refinery for providing the sludge sample.

References

[1] Hu G, Li J, Zeng G. Recent development in the treatment of oily sludge from petroleum industry: a review. J Hazard Mater 2013;261:470–90.
[2] Matsui T, et al. Degradation of oil tank sludge using long-chain alkane-degrading bacteria. Ann Microbiol 2014;64(1):391–5.
[3] Adetutu E, et al. Exploiting the intrinsic hydrocarbon-degrading microbial capacities in oil tank bottom sludge and waste soil for sludge bioremediation. Int J Environ Sci Technol 2015;12(4):1427–36.
[4] Huang Q, et al. Characterization of emulsified water in petroleum sludge. Fuel 2014;118:214–9.

[5] Hu G, et al. Investigation of waste biomass co-pyrolysis with petroleum sludge using a response surface methodology. J Environ Manage 2017;192:234–42.
[6] Cheng S, et al. Evaluation of oil sludge ash as a solid heat carrier in the pyrolysis process of oil sludge for oil production. Energy Fuels 2016;30(7):5970–9.
[7] Wang S, et al. Bioremediation of oil sludge contaminated soil by landfarming with added cotton stalks. Int Biodeterior Biodegrad 2016;106:150–6.
[8] Hou B, et al. The treatment of refinery heavy oil sludge. Pet Sci Technol 2013;31(5):458–64.
[9] Egazar'yants S, et al. Oil sludge treatment processes. Chem Technol Fuels Oils 2015;51(5):506–15.
[10] Hu G, et al. Ultrasonic oil recovery and salt removal from refinery tank bottom sludge. J Environ Sci Health Part A 2014;49(12):1425–35.
[11] Silva D, et al. Production of oil with potential energetic use by catalytic co-pyrolysis of oil sludge from offshore petroleum industry. J Anal Appl Pyrol 2017;124:290–7.
[12] Huang Q, et al. Migration of emulsified water droplets in petroleum sludge during centrifugation. Energy Fuels 2014;28(8):4918–24.
[13] Huang Q, et al. Effect of the particle surface on oil recovery from petroleum sludge. Energy Fuels 2014;28(7):4480–5.
[14] Hu G, et al. Oil recovery from petroleum sludge through ultrasonic assisted solvent extraction. Journal of Environmental Science and Health, Part A 2016;51(11):921–9.
[15] Huang Q, et al. Catalytic pyrolysis of petroleum sludge for production of hydrogen-enriched syngas. Int J Hydrogen Energy 2015;40(46):16077–85.
[16] Liu J, et al. Pyrolysis treatment of oil sludge and model-free kinetics analysis. J Hazard Mater 2009;161(2–3):1208–15.
[17] Schmidt H, Kaminsky W. Pyrolysis of oil sludge in a fluidised bed reactor. Chemosphere 2001;45(3):285–90.
[18] Shie J-L, et al. Pyrolysis of oil sludge with additives of catalytic solid wastes. J Anal Appl Pyrol 2004;71(2):695–707.
[19] Cheng S, et al. Pyrolysis of oil sludge with oil sludge ash additive employing a stirred tank reactor. J Anal Appl Pyrol 2016;120:511–20.
[20] Cheng S, et al. Effect of steam and oil sludge ash additive on the products of oil sludge pyrolysis. Appl Energy 2017;185:146–57.
[21] Shie J-L, et al. Use of inexpensive additives in pyrolysis of oil sludge. Energy Fuels 2002;16(1):102–8.
[22] Shie J-L, et al. Pyrolysis of oil sludge with additives of sodium and potassium compounds. Resour Conserv Recycl 2003;39(1):51–64.
[23] Xu X, et al. Co-pyrolysis characteristics of municipal sewage sludge and hazelnut shell by TG-DTG-MS and residue analysis. Waste Manage 2017;62:91–100.
[24] Alvarenga LM, et al. Determination of activation energy of pyrolysis of carton packaging wastes and its pure components using thermogravimetry. Waste Manage 2016;53:68–75.
[25] Hu M, et al. Kinetic study and syngas production from pyrolysis of forestry waste. Energy Convers Manage 2017;135:453–62.
[26] Fernandez A, et al. Kinetic study of regional agro-industrial wastes pyrolysis using non-isothermal TGA analysis. Appl Therm Eng 2016;106:1157–64.
[27] Liu G, Song H, Wu J. Thermogravimetric study and kinetic analysis of dried industrial sludge pyrolysis. Waste Manage 2015;41:128–33.
[28] Bosmans A, De Dobbelaere C, Helsen L. Pyrolysis characteristics of excavated waste material processed into refuse derived fuel. Fuel 2014;122:198–205.
[29] Singh RK, Ruj B. Time and temperature depended fuel gas generation from pyrolysis of real world municipal plastic waste. Fuel 2016;174:164–71.
[30] Gai C, Dong Y, Zhang T. The kinetic analysis of the pyrolysis of agricultural residue under non-isothermal conditions. Bioresour Technol 2013;127:298–305.
[31] Chen S, et al. TGA pyrolysis and gasification of combustible municipal solid waste. J Energy Inst 2015;88(3):332–43.
[32] Punnaruttanakun P, et al. Pyrolysis of API separator sludge. J Anal Appl Pyrol 2003;68:547–60.
[33] Wang Z, et al. Low temperature pyrolysis characteristics of oil sludge under various heating conditions. Energy Fuels 2007;21(2):957–62.
[34] Karayildirim T, et al. Characterisation of products from pyrolysis of waste sludges. Fuel 2006;85(10–11):1498–508.
[35] Cheng S, et al. Progress in thermal analysis studies on the pyrolysis process of oil sludge. Thermochim Acta 2018;663:125–36.
[36] Mishra RK, Mohanty K, Wang X. Pyrolysis kinetic behavior and Py-GC–MS analysis of waste dahlia flowers into renewable fuel and value-added chemicals. Fuel 2020;260:116338.
[37] Özsin G, Pütün AE, Pütün E. Investigating the interactions between lignocellulosic biomass and synthetic polymers during co-pyrolysis by simultaneous thermal and spectroscopic methods. Biomass Convers Biorefin 2019;9(3):593–608.
[38] Barzegar R, et al. TGA and kinetic study of different torrefaction conditions of wood biomass under air and oxy-fuel combustion atmospheres. J Energy Inst 2019.
[39] Özsin G, et al. A thermo-kinetic study on co-pyrolysis of oil shale and polyethylene terephthalate using TGA/FT-IR. Korean J Chem Eng 2020:1–11.
[40] Friedman HL. Kinetics of thermal degradation of char-forming plastics from thermogravimetry. Application to a phenolic plastic. in Journal of Polymer Science Part C: Polymer Symposia. 1964. Wiley Online Library.
[41] Ozawa T. A new method of analyzing thermogravimetric data. Bull Chem Soc Jpn 1965;38(11):1881–6.
[42] Flynn JH, Wall LA. General treatment of the thermogravimetry of polymers. J Res Nat Bur Stand 1966;70(6):487–523.
[43] Kissinger HE. Reaction kinetics in differential thermal analysis. Anal Chem 1957;29(11):1702–6.
[44] Akahira T, Sunose T. Method of determining activation deterioration constant of electrical insulating materials. Res Rep Chiba Inst Technol (Sci Technol) 1971;16:22–31.
[45] Starink M. A new method for the derivation of activation energies from experiments performed at constant heating rate. Thermochim Acta 1996;288(1–2):97–104.
[46] Tang W, et al. New approximate formula for Arrhenius temperature integral. Thermochim Acta 2003;408(1–2):39–43.
[47] Vlaev LT, Georgieva VG, Tavlieva MP. On the kinetic mechanism of non-isothermal degradation of solids. In: Reactions and Mechanisms in Thermal Analysis of Advanced Materials. Hoboken, NJ, USA: Wiley; 2015. p. 547–78.
[48] Chen Z, et al. Preparation of LiZnPO4· H2O via a novel modified method and its non-isothermal kinetics and thermodynamics of thermal decomposition. J Therm Anal Calorim 2012;108(3):1235–42.
[49] Long Q, et al. Facile synthesis of hydrotalcite and its thermal decomposition kinetics mechanism study with masterplots method. Thermochim Acta 2014;579:50–5.
[50] Genieva S, et al. Kinetic analysis and pyrolysis mechanism of raw and impregnated almond shells. Thermochim Acta 2021;698:178877.
[51] Loy ACM, et al. Thermogravimetric kinetic modelling of in-situ catalytic pyrolytic conversion of rice husk to bioenergy using rice hull ash catalyst. Bioresour Technol 2018;261:213–22.
[52] Xu F-X, et al. TG-FTIR for kinetic evaluation and evolved gas analysis of cellulose with different structures. Fuel 2020;268:117365.
[53] Barzegar R, et al. TGA and kinetic study of different torrefaction conditions of wood biomass under air and oxy-fuel combustion atmospheres. J Energy Inst 2020;93(3):889–98.
[54] Zhao M, et al. Iso-conversional kinetics of low-lipid micro-algae gasification by air. J Cleaner Prod 2019;207:618–29.
[55] Özsin G. Assessing thermal behaviours of cellulose and poly (methyl methacrylate) during co-pyrolysis based on an unified thermoanalytical study. Bioresour Technol 2020;300:122700.
[56] Manić N, Janković B, Dodevski V. Model-free and model-based kinetic analysis of Poplar fluff (Populus alba) pyrolysis process under dynamic conditions. J Therm Anal Calorim 2020:1–20.
[57] Qu Y, et al. Kinetic study of the effect of in-situ mineral solids on pyrolysis process of oil sludge. Chem Eng J 2019;374:338–46.
[58] Shie JL, et al. Resources recovery of oil sludge by pyrolysis: kinetics study. J Chem Technol Biotechnol 2000;75(6):443–50.
[59] Choudhury D, et al. Non-isothermal thermogravimetric pyrolysis kinetics of waste petroleum refinery sludge by isoconversional approach. J Therm Anal Calorim 2007;89(3):965–70.
[60] Dhyani V, Kumar J, Bhaskar T. Thermal decomposition kinetics of sorghum straw via thermogravimetric analysis. Bioresour Technol 2017;245:1122–9.
[61] Shahbeig H, Nosrati M. Pyrolysis of municipal sewage sludge for bioenergy production: Thermo-kinetic studies, evolved gas analysis, and techno-socio-economic assessment. Renew Sustain Energy Rev 2020;119:109567.
[62] Zhang Z, et al. Investigation of kinetic compensation effect in lignocellulosic biomass torrefaction: Kinetic and thermodynamic analyses. Energy 2020;207:118290.
[63] Zsakó J. The kinetic compensation effect. J Therm Anal 1976;9(1):101–8.
[64] Janković B. The pyrolysis of coffee paper cup waste samples using non-isothermal thermo-analytical techniques. The use of combined kinetic and statistical analysis in the interpretation of mechanistic features of the process. Energy Convers Manage 2014;85:33–49.
[65] Ahmad MS, et al. A modified DAEM: To study the bioenergy potential of invasive Staghorn Sumac through pyrolysis, ANN, TGA, kinetic modeling, FTIR and GC–MS analysis. Energy Convers Manage 2020;221:113173.
[66] Rasam S, et al. Thermal behavior, thermodynamics and kinetics of co-pyrolysis of binary and ternary mixtures of biomass through thermogravimetric analysis. Fuel 2020;280:118665.
[67] Tabal A, Barakat A, Aboulkas A. Pyrolysis of ficus nitida wood: Determination of kinetic and thermodynamic parameters. Fuel 2021;283:119253.
[68] Zhao S, et al. Kinetics and thermodynamics evaluation of carbon dioxide enhanced oil shale pyrolysis. Sci Rep 2021;11(1):1–14.
[69] Merdun H, Laougé ZB. Kinetic and thermodynamic analyses during co-pyrolysis of greenhouse wastes and coal by TGA. Renew Energy 2021;163:453–64.
[70] Kaur R, et al. Pyrolysis kinetics and thermodynamic parameters of castor (Ricinus communis) residue using thermogravimetric analysis. Bioresour Technol 2018;250:422–8.
[71] Ding G, et al. Synergistic effect, kinetic and thermodynamics parameters analyses of co-gasification of municipal solid waste and bituminous coal with CO2. Waste Manage 2021;119:342–55.
[72] Tahir MH, et al. Pyrolysis of oil extracted safflower seeds: product evaluation, kinetic and thermodynamic studies. Bioresour Technol 2020;314:123699.
[73] Özsin G, Pütün AE. Kinetics and evolved gas analysis for pyrolysis of food processing wastes using TGA/MS/FT-IR. Waste Manage 2017;64:315–26.
[74] Polat S, Apaydin-Varol E, Pütün AE. Thermal decomposition behavior of tobacco stem Part I: TGA–FTIR–MS analysis. Energy Sources Part A 2016;38(20):3065–72.